PNAS
www.pnas.org

Supplementary Information for

Holographic Acoustic Tweezers

Asier Marzo, Bruce W. Drinkwater

Asier Marzo
Email: amarzo@hotmail.com

This PDF file includes:

Materials and Methods
Figs. S1 to S22
Captions for movies S1 to S8

Other supplementary materials for this manuscript include the following:

Movies S1 to S8

www.pnas.org/cgi/doi/10.1073/pnas.1813047115

Materials and Methods

Particle Placement

We manually loaded the particles into an initial configuration using physical tweezers. It was easy to place the particles at the right position since in the initial configuration all the particles started in a horizontal plane at a known height (as in the beginning of Movie S1). Also, the converging forces can attract the particles from up to 2 cm away laterally (X-Y plane) so it is not necessary to place the particle in the exact initial positions. Alternatively, we used a semi-automatic approach. An acoustically-transparent grid was placed 3 cm above the bottom array. The grid had small indents where the particles were placed. These initial positions were known in the control software, so it was possible to automatically pick them up and move them to the target positions.

Positioning Accuracy

To obtain an estimation of the repositioning accuracy, an animation (as shown in Movie S2) was played forwards while pictures were taken from a camera at certain frames of the animation, then the animation was played backwards, and another set of pictures was taken with the camera (Canon EOS 550d) in the same position. The centre of the particles was extracted from the pictures and the distance between centres of similar frames was calculated. This process was repeated once more with the camera pointing from a perpendicular position to the original one. A ruler in the centre parallel to the camera was used to transform from pixels to mm. The positioning errors were obtained in the camera planes space and were similar in both axes and views. The repositioning accuracy of the particles was ± 0.1mm ($\lambda/86$) for the in-plane and ±0.5mm ($\lambda/17$) for the 3D manipulation.

Experimental Trapping Force Measurement

Experiments were conducted to measure the trapping force and validate that trends predicted by the simulations (i.e. trapping forces being inversely and linearly proportional to the number of traps). Also, the absolute force values should be within the same order of magnitude in simulations and experiments. Trapping of 1, 2, 3 and 4 particles forming a square of 5 cm side placed at the centre of two opposed arrays was experimentally tested. We employed two methods to experimentally measure the trapping forces:
a) The drop test[1,2] in which the voltage sent to the emitters is reduced until the particles fall. The voltage is proportional to the amplitude of the generated field, and the square of the amplitude is proportional to the exerted force. Thus, the minimum voltage required to levitate can reveal the exerted forces. For this experiment we levitated a droplet of water (density 1000 kg/m^3) of approximately 1.2 mm diameter. The exact size of the levitated particle is not relevant since the radiation force is proportional to the volume and so is the weight; therefore, density is the determining factor. The relative results are shown in Figure S13.a, the experiment follows the same trend as the simulations regarding the force being inversely linearly proportional to the number of traps. The experiments (4 repetitions) required excitation voltages of 5.27 V SD=0.15 V, 7.05 V SD=0.43 V, 8.4 V SD=0.07 V, and 9.75 V SD=0.23 V for 1, 2, 3 and 4 traps respectively. The required simulated voltages were 4.00 V, 5.56V, 6.61V, and 7.59V. 50% errors can be expected from the dropping test test[1,2] thus our error of 25% is within normal range.

b) Force stiffness from particle oscillation frequency[3]. When the particles are moved from one position to another they oscillate following a damped harmonic oscillator model due to the converging trapping forces. The natural frequency of the oscillation can be used to approximate the spring trapping stiffness. We used 2 mm diameter particles made of EPS (29 kg/m^3). The relative results are shown in Figure S13.b. The experimental (4 repetitions) trapping stiffness along the x-direction was 5.07 mN/m SD=0.05 mN/m, 2.51 mN/m SD=0.07 mN/m, 1.72 mN/m SD=0.05 mN/m, and 1.26 mN/m SD=0.08 mN/m for 1, 2, 3 and 4 traps respectively whereas the simulated stiffnesses were 9.79 mN/m, 4.21 mN/m, 3.17 mN/m, and 2.33 mN/m. The error is 58% potentially due to inaccuracy in the measurement of the density and size of the particles.

Incident Acoustic Field

We model the emission of the transducers as single-frequency piston sources[4]. The complex acoustic pressure P_l at point $\boldsymbol{r}$ generated by a piston source l can be modelled as:

$$P_l\boldsymbol{r}) = P_0 A \frac{D_f(\theta)}{d} e^{i(\varphi + kd)}$$

Where P_0 is a transducer efficiency constant and A is the peak-to-peak voltage used to excite the emitters. D_f is a far-field directivity function that depends on the angle θ between the transducer normal and $\boldsymbol{r}$. Here, $D_f = 2J_1(ka\sin\theta)/ka\sin\theta$, which is the directivity function of a circular piston source, where J_1 is a first order Bessel function of the first kind and a is the piston radius. d is the propagation distance in free space. $k = 2\pi/\lambda$ is the wavenumber and λ is the wavelength (8.6 mm in air at 25 °C). φ is the initial phase of the piston. For an array of multiple piston sources, the total field can be obtained by summation of the contribution from each source $P = \sum P_l$.
For the transducers employed (i.e. MA40S4S), $P_0 = 0.17\ Pa$ at 1 meter per *Vpp* of a square excitation signal, and $a = 4.5\ mm$ to match the manufacturers stated directivity.

Radiation Force on a Particle

To calculate the force exerted on a sphere significantly smaller than the wavelength due to a complex pressure field, we use the negative gradient of the Gor'kov potential[5,6] $\boldsymbol{F} = -\boldsymbol{\nabla} U$:

$$U = 2K_1(|p|^2) - 2K_2(|p_x|^2 + |p_y|^2 + |p_z|^2)$$

$$K_1 = \frac{1}{4}V\left(\frac{1}{c_0^2\rho_0} - \frac{1}{c_s^2\rho_s}\right)$$

$$K_2 = \frac{3}{4}V\left(\frac{\rho_0 - \rho_s}{\omega^2\rho_0(\rho_0 + 2\rho_s)}\right)$$

where V is the volume of the spherical particle, ω is the frequency of the emitted waves, ρ is the density and c is the speed of sound (subscripts *0* and *s* referring to the host medium and the solid particle material respectively). p is the complex pressure and p_x, p_y, p_z are its spatial derivates over *x*, *y* and *z*. Air host medium, $\rho_0 = 1.18\ kg/m^3$ and $c_0 = 346\ m/s$. Expanded Polystyrene (EPS) particles $\rho_s = 29\ kg/m^3$ and $c_s = 900\ m/s$

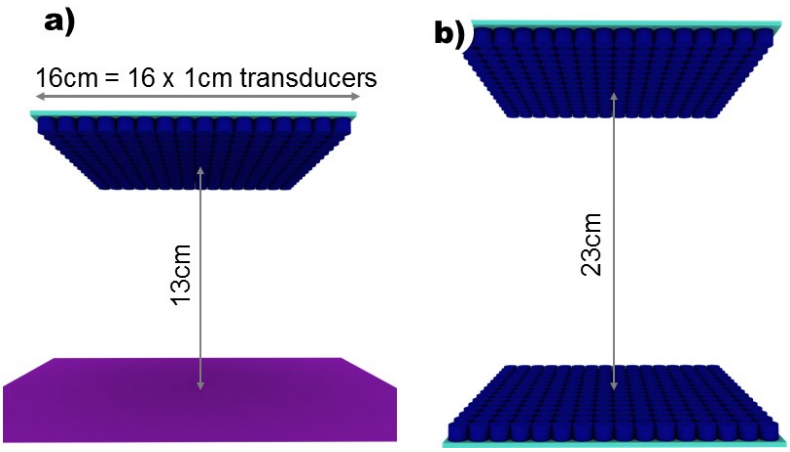

Fig. S1: Array geometries employed for HAT. The arrays are made of 16x16 arrays with 1cm (1.2λ) diameter transducer elements arranged on a 1cm grid and operating at 40kHz in air. a) a single array parallel to an acoustically reflective surface separated by 13cm (15.1λ). b) two opposed arrays separated by 23 cm (26.7λ).

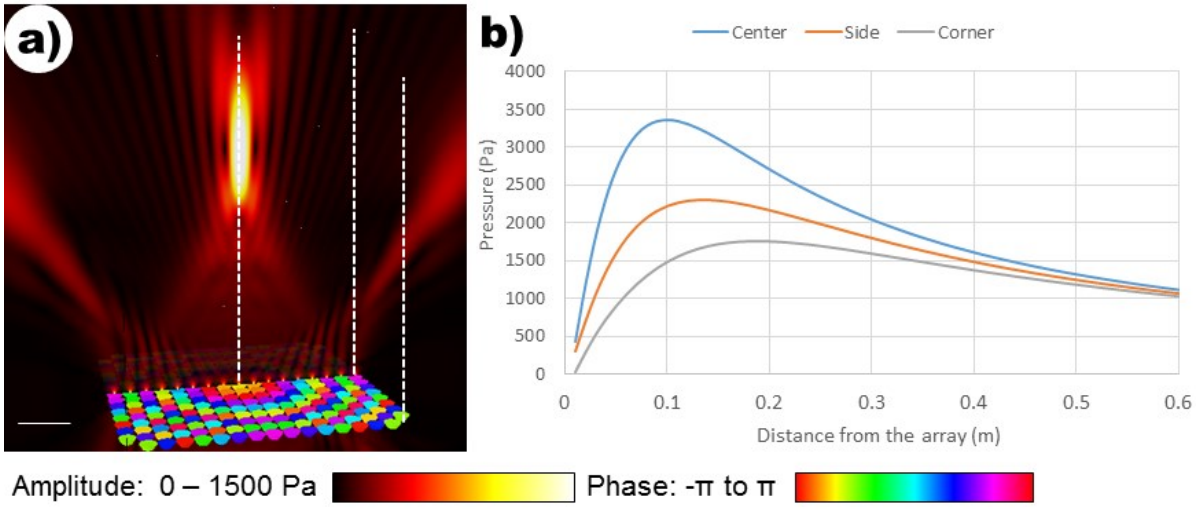

Fig. S2: a) Simulated acoustic pressure amplitude due to a focal point generated 11.6λ (10cm) above the array, scale bar in (a) is 3cm. b) Simulated acoustic pressure amplitude of a focal point at different distances at the centre, side and corner of the array. The peak pressure occurs in the region 10-18cm. This range of distances was used to choose the separation between the array and the reflective surface as well as the distance to the centre of the two opposed arrays.

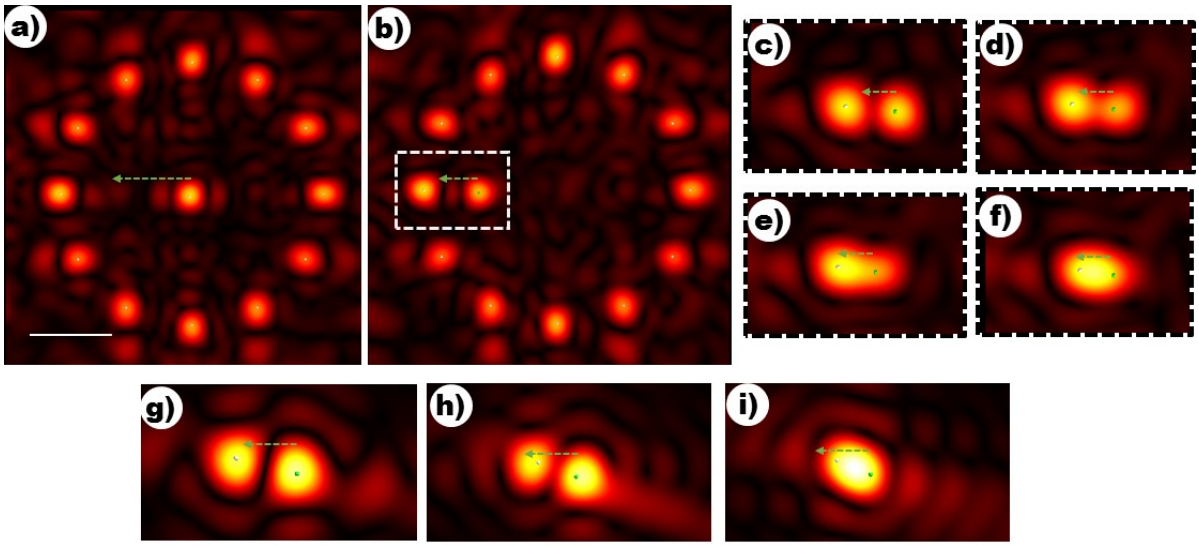

Fig. S3: Simulated acoustic pressure amplitude of multiple foci in the reflective plane when generated by an array 15.1λ (13cm) above the reflective plane. In (a-f), 13 focal points are generated and the central one is moved progressively towards the left. (c-f) are close-ups of (b). In (d) the target positions the focal points start to interfere, in (e,f) the focal points have fused in to a single focus. In (g-i) only 2 focal points are generated and moved together. In all cases, the minimum distance before interference became apparent was ≈1.3cm or 1.5λ. The scale (a) represents 2cm.

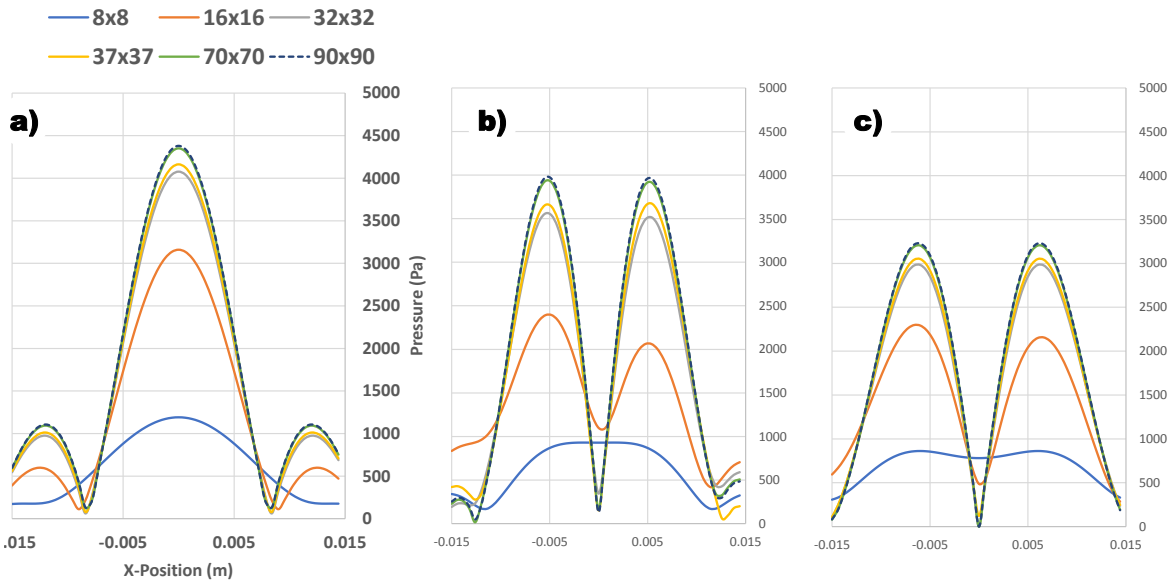

Fig. S4: Simulated acoustic pressure amplitude along the x-direction through the focal points for a 16x16cm array focused at two points 15.1λ (13cm) above the array with each point separated by: a) 5mm, b) 8.5mm (Rayleigh criterion) and c) 14mm. The results are shown for arrays with different numbers of emitting elements (8x8, 16x16x, 32x32, 37x37, 70x70 and 90x90 elements). The two focal points can only be generated correctly if the separation of the foci is larger than 10mm and the element pitch is smaller than λ/2

(i.e. 37 or more elements). Element pitches smaller than λ/2 do not improve the resolution.

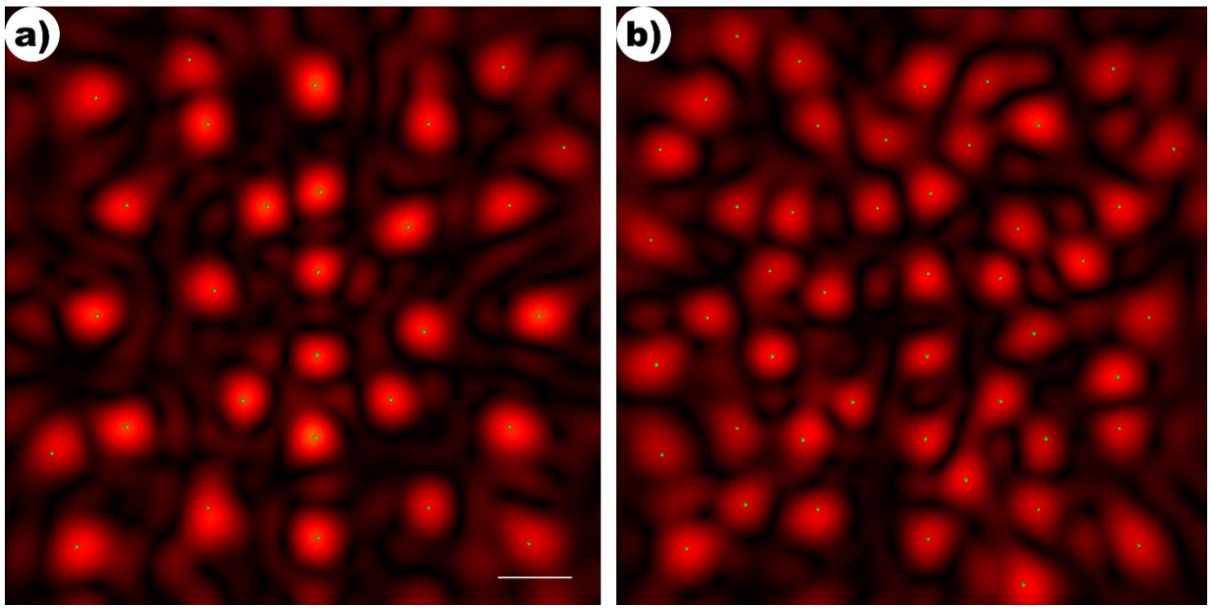

Fig. S5*:* Simulated acoustic pressure amplitude for foci at the reflective plane using a parallel 16x16 array 15.1λ (13cm) above the reflective plane. The slices are 16x16 cm in size. a) 28 focal points, the amplitudes at the focal points/traps are always larger than that appearing away from the traps. b) 48 focal points, the amplitude at some focal points is no larger than that at undesired locations. The scale (a) represents 2cm.

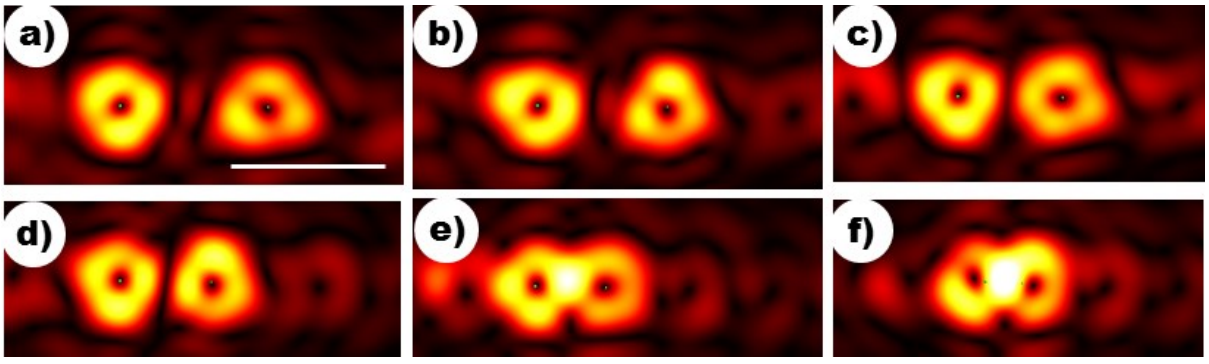

Fig. S6: Simulated acoustic pressure amplitude for two vortices at the reflective plane using a 16x16 array 15.1λ (13cm) above the reflective plane. The minimum distance between the vortices cores was ≈1.4cm (1.6λ) as can be seen in (e) the target points are in the cores whereas in (f) the cores cannot follow the target points. Scale bar (a) is 2 cm.

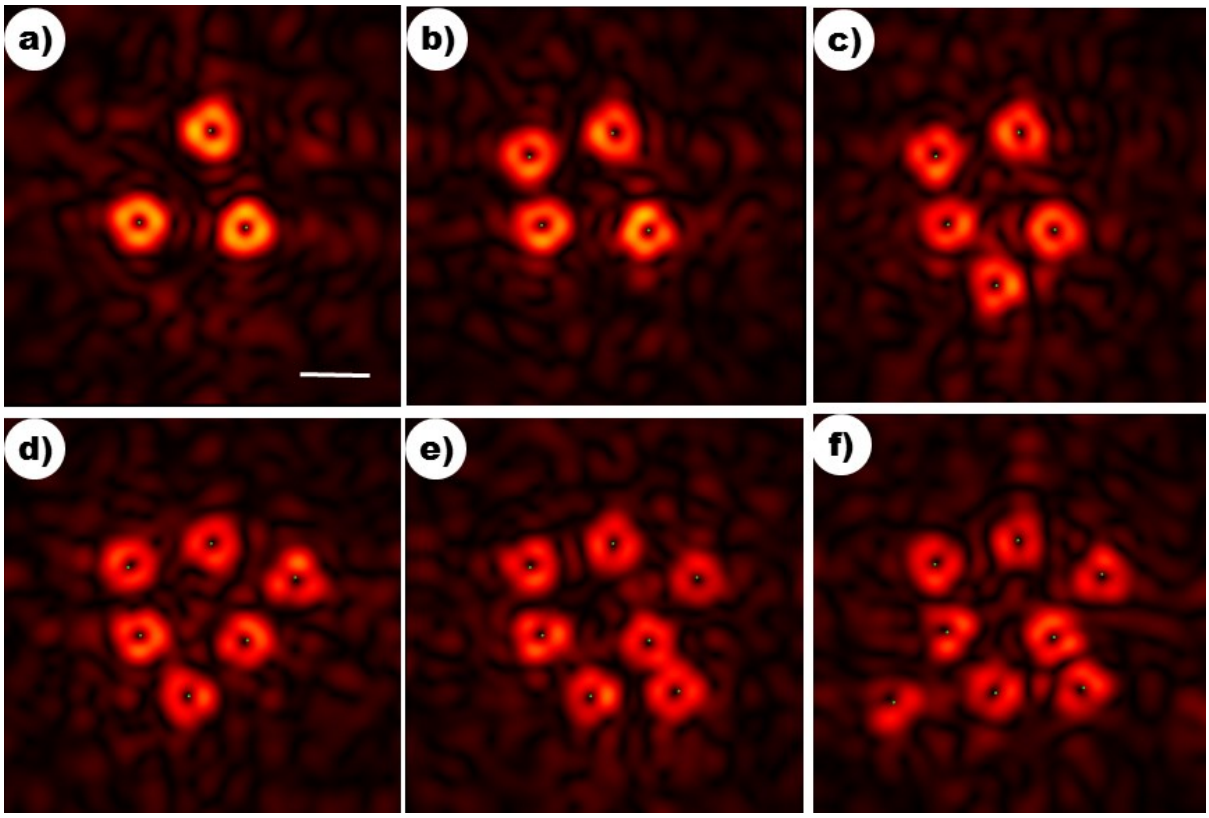

Fig. S7: Simulated acoustic pressure amplitude in the reflective plane for different numbers of vortices using a parallel 16x16 array 15.1λ (13cm) above the reflective plane. Beyond 5 vortices (d-f), the vortex rings started to interfere and lose definition. Scale bar (a) is 2 cm.

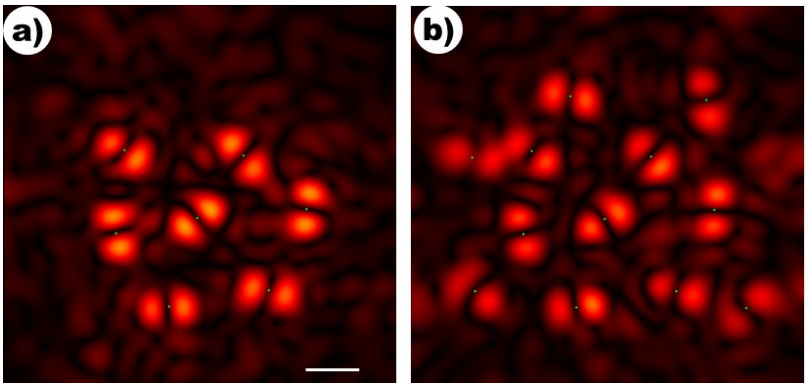

Fig. S8: Simulated pressure amplitude field in the reflective plane for different numbers of twin-traps generated using a parallel 16x16 array 15.1λ (13cm) above the reflective plane. Beyond 7 twin-traps the traps start to lose definition. a) 7 twin-traps with different orientations. b)12 twin-traps. Scale bar is 2 cm.

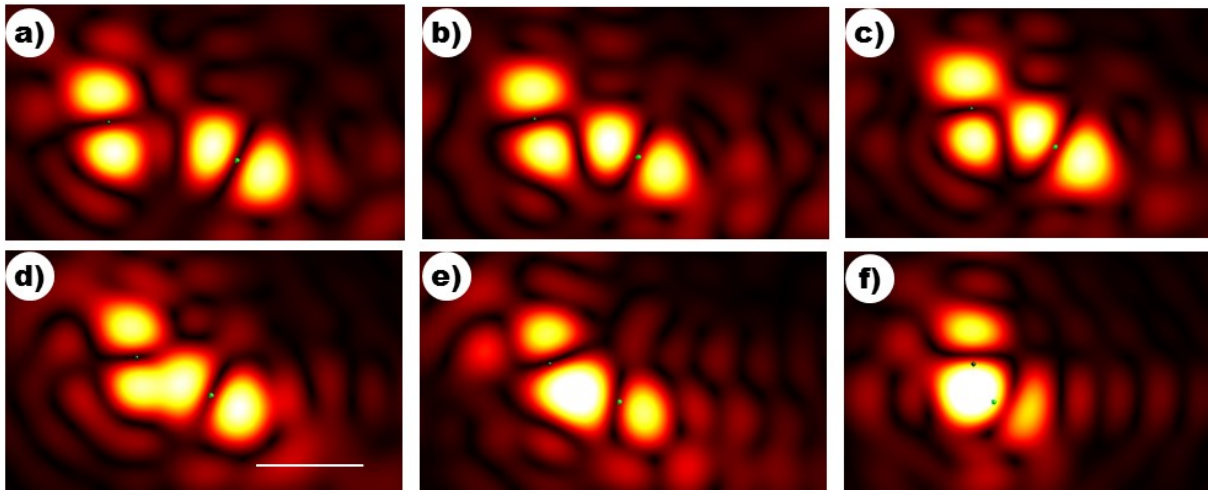

Fig. S9: Simulated acoustic pressure amplitude in the reflective plane for two twin-traps generated using a parallel 16x16 array 15.1λ (13cm) above the reflective plane. The minimum distance between the twin-traps was found to be ≈1.7cm (1.4λ). Scale bar is 2 cm.

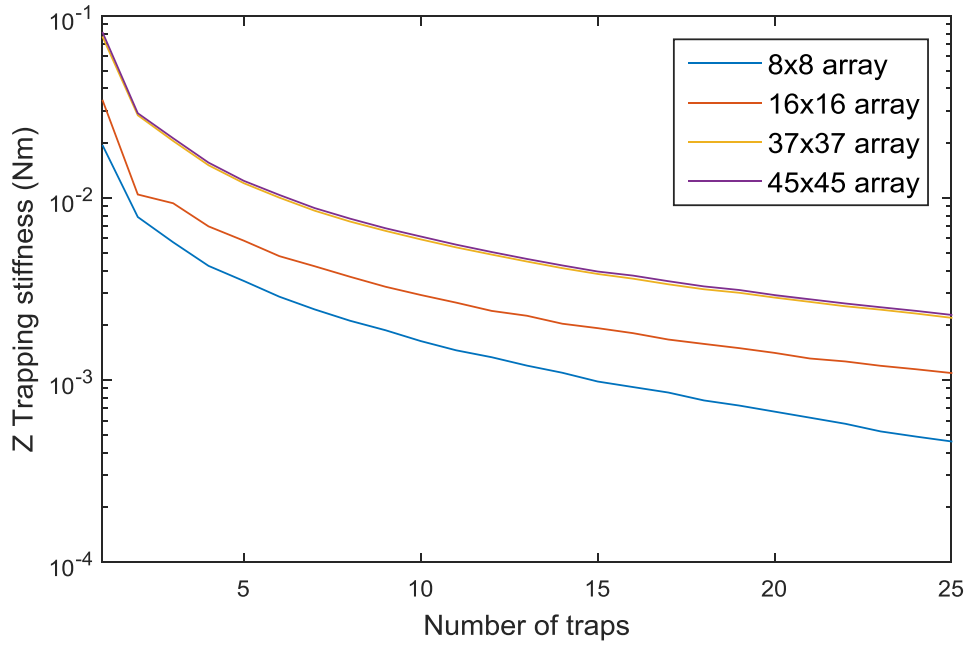

Fig. S10: Simulated trapping stiffness in the Z-direction depending on the number of traps and elements of a 16x16cm array (8x8, 16x16x, 37x37 and 45x45 elements). Percentile 95 is shown from 1000 instances of traps generated randomly in a 12x12x12 cm cube at the centre of two opposed arrays (minimum distance between points of 2cm). Note that after 37x37 there is no further improvement since the element pitch is already smaller than λ/2. The x and y force stiffnesses followed similar patterns.

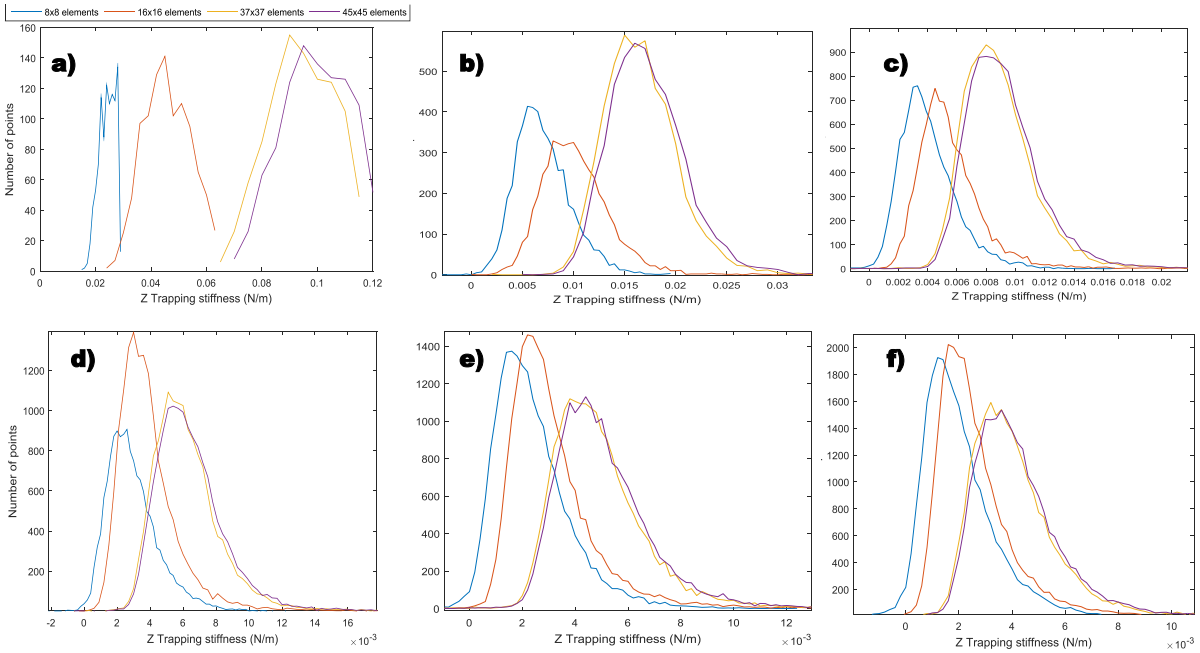

Fig. S11: Simulated trapping stiffness in the Z-direction depending on the number of traps and elements of a 16x16cm array (8x8, 16x16x, 37x37, 45x45 elements). Histograms of 1000 instances of traps generated randomly in a 12x12x12 cm cube at the centre of two opposed arrays separated by 23cm (minimum distance between foci of 2cm). a) 1 trap. b) 5 traps. c) 10 traps. d) 15 traps. e) 20 traps. f) 25 traps. The x and y force stiffnesses followed similar patterns.

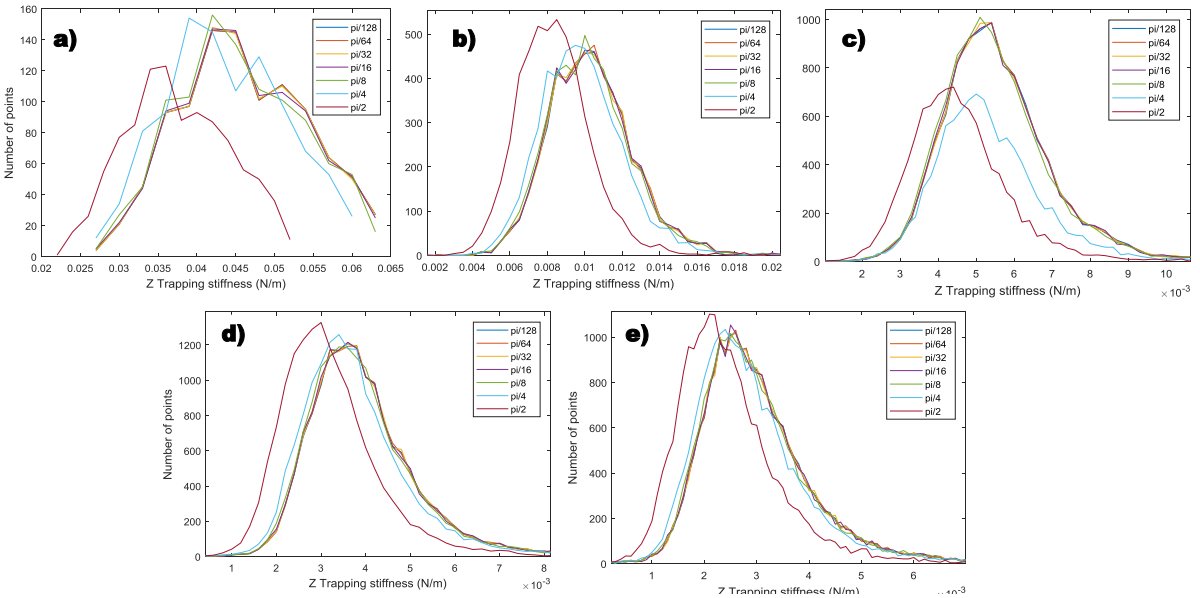

Fig. S12: Simulated trapping stiffness in the Z-direction depending on the number of traps and phase resolution (π/128, π/64, π/32, π/16, π/8, π/4 and π/2 radians). Histograms of 1000 instances of traps generated randomly in a 12x12x12 cm cube at the centre of two opposed arrays (16x16 with 1 cm elements and pitch) separated by 23cm (minimum distance between points of 2cm). a) 1 trap. b) 5 traps. c) 10 traps. d) 15 traps. e) 20 traps. The x and y force stiffnesses followed similar patterns. There is a significant

improvement from π/2 to π/4 radians but beyond that point the stiffnesses show only small changes.

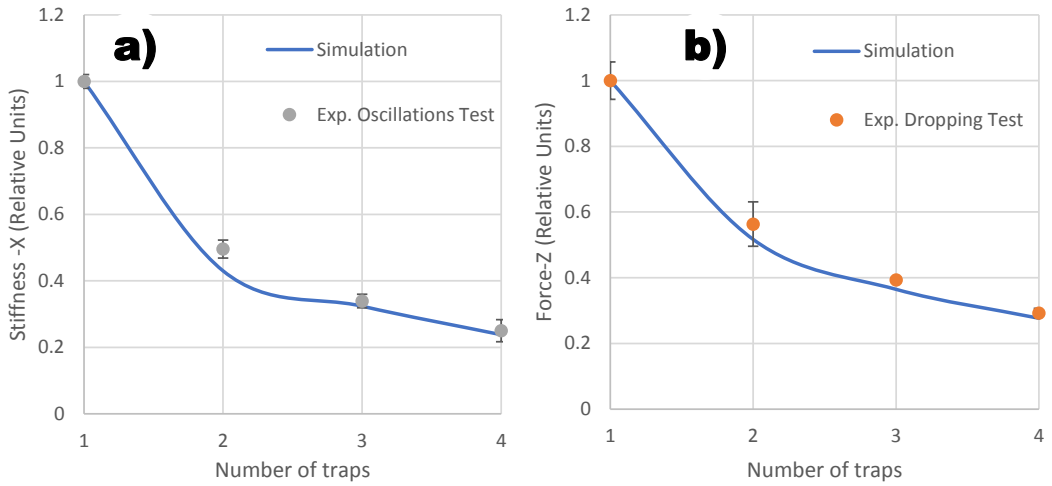

Fig. S13: Relative Trapping Forces and Stiffness for different numbers of traps. The setup was the two-opposed-arrays system (Fig. S1.b) and the traps were created in the centre forming a square in the XY plane with a side of 5 cm. The reported values are relative to the force or stiffness obtained with 1 trap. The experiments were repeated 3 times and the error bars represent the standard deviation. a) stiffness in the x-direction obtained from observation of particle oscillation and b) force in the z-direction obtained from the dropping test.

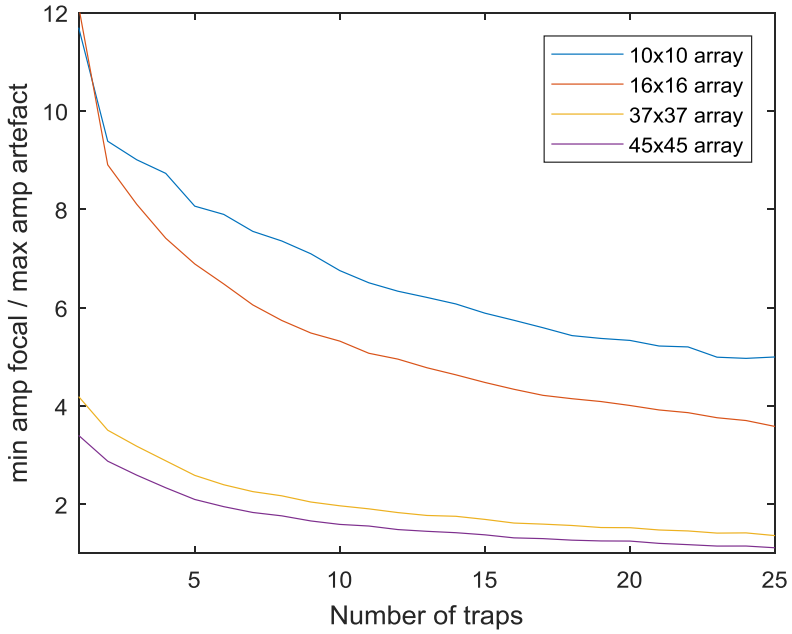

Fig. S14: Ratio of minimum amplitude of all the focal points divided by the maximum amplitude of all the artefacts. Results are the average of 500 instances in which a 16x16

cm array of different numbers of elements generate focal points 13 cm above its centre into a 12x12 cm slice.

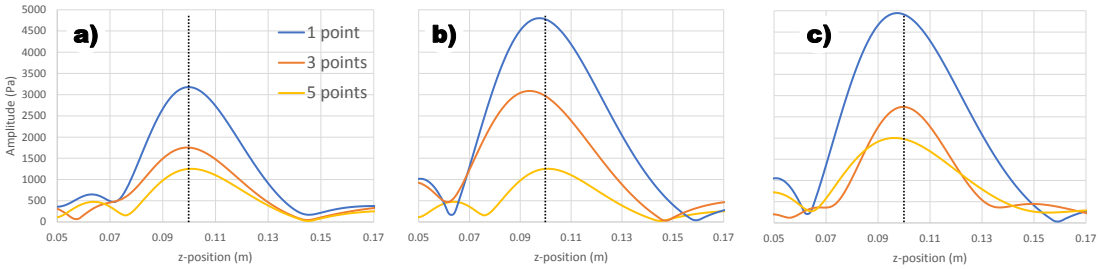

Fig. S15: Simulated acoustic pressure amplitude along the z-axis of an array of 16x16 cm focused 10 cm above its centre. "1 point" represents only a single focal point, "3 points" have additional focal points at both sides of the central focal point, and "5 points" has 2 at each side. a) 16x16 elements, b) 32x32 elements, c) 45x45 elements.

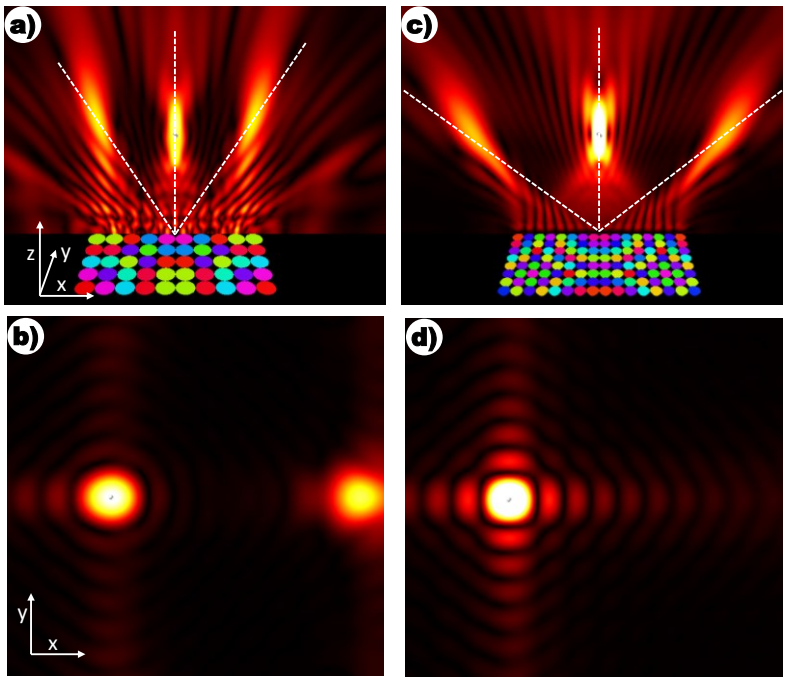

Fig. S16: Slices of 16x16 cm for the simulated acoustic pressure amplitude of arrays focused 10 cm above them. a,b) 10x10 element array. c,d) 16x16 element array. The array with less elements has less intense artefacts (b,d) but the main sidelobes are located closer to the center (a,c).

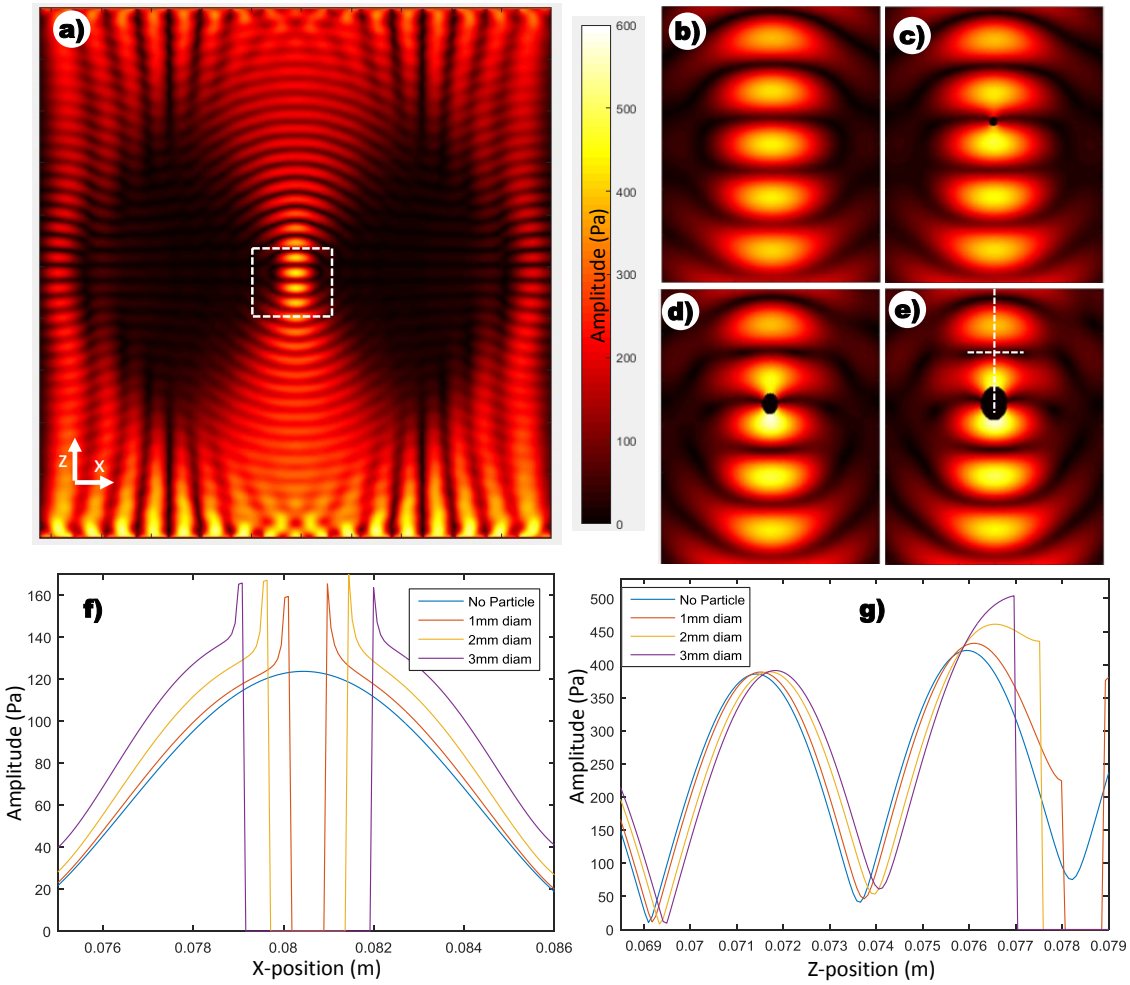

Fig. S17: a) Acoustic pressure amplitude calculated using a 2D FDTD model that includes the reflections from the particle. The simulation is for the two opposed arrays of 16 elements, they are focused in the centre and the slice is 16x16 cm. b) zoomed-in field with no particle, c) 1mm diameter particle, d) 2mm, and e) 3mm. f) Amplitude line along the x-axis and (g) z-axis, the lines are marked in (e). A 1mm particle produces minimum deviations in the field whereas the deviations caused by a 3mm diameter particle are more significant.

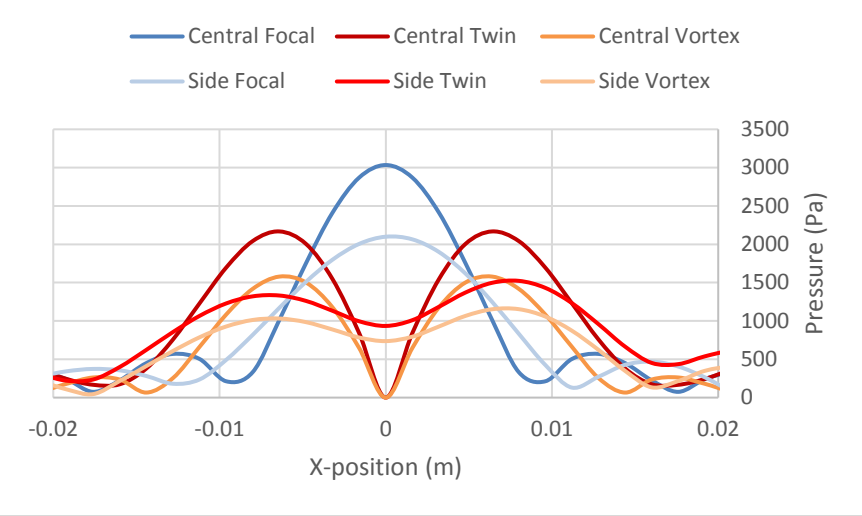

Fig. S18: Simulated acoustic pressure amplitude distribution of different traps at the centre of the HAT device (as per Fig. S1.a) and at the side.

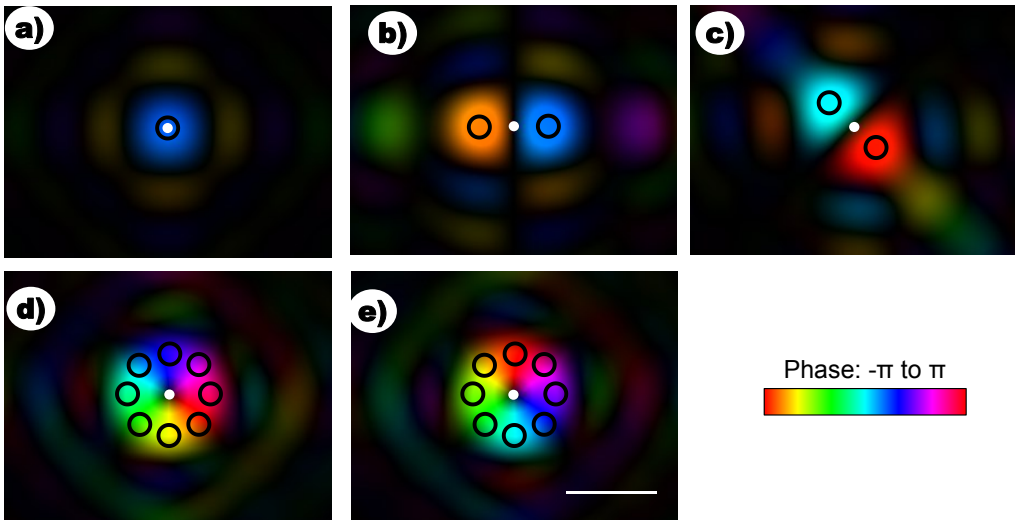

Fig. S19: Location of control points for various traps. a) a focal point requires a single control point. b,c) a twin-trap has two control points separated by 1.4λ and with a π radians offset between the points. d) clockwise vortex has 8 points in a circle separated 1.4λ and with an increasing phase from 0 to 2 π. e) counter-clockwise vortex, reverses the ordering of the phases. b) is in the XZ-plane whereas the other slices are in the XY-plane.

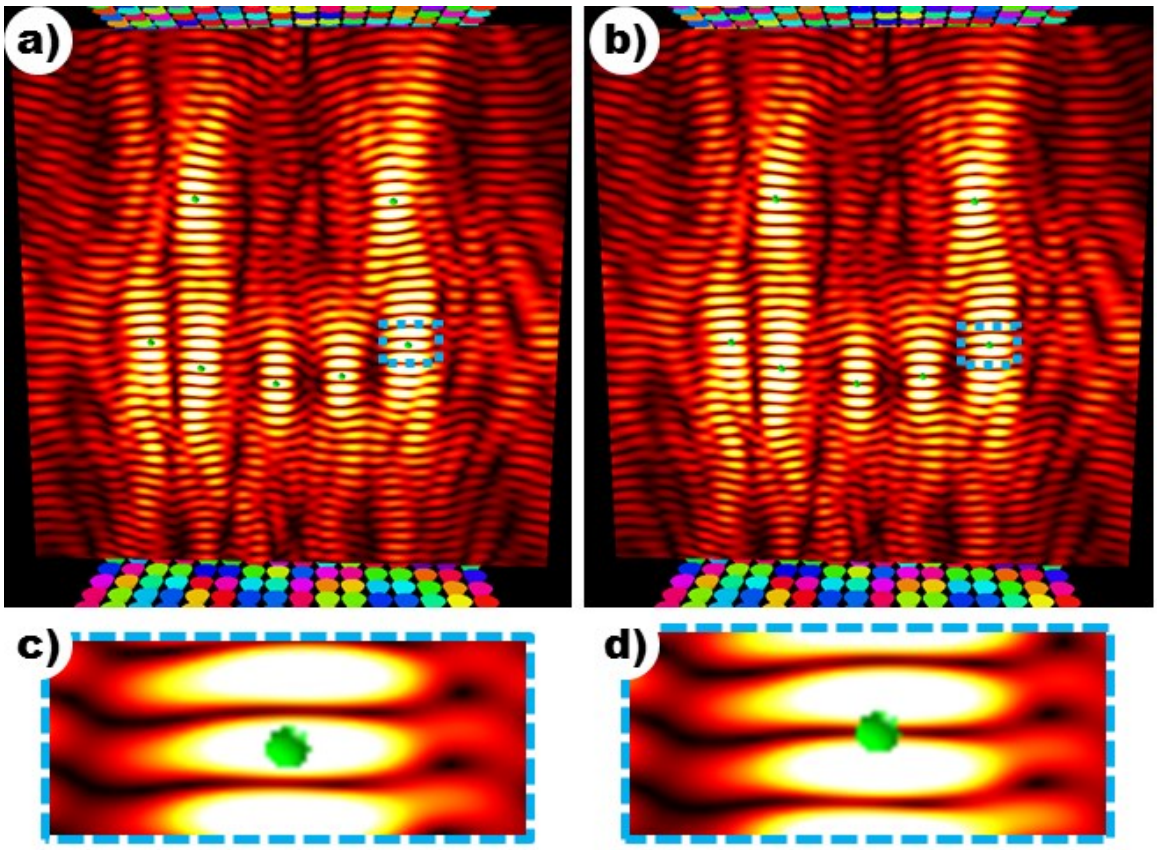

Fig. S20: Simulated acoustic pressure amplitude in the XZ plane of multiple traps generated between two opposed arrays (as per Fig. S1.b) by (a) focusing on the target points and (b) adding π radians to the phase of the top array. (c) is a zoom-in on the simulated pressure amplitude field (a) whereas (d) is a zoom-in on the field (b).

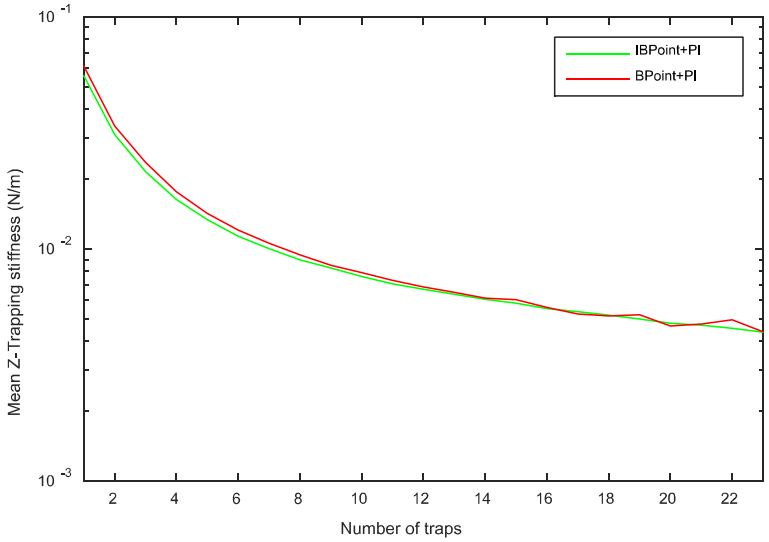

Fig. S21: Simulated mean trapping stiffness in the Z-direction depending on the number of traps and employed algorithm. Shown here is the 95th percentile of 1000 instances of traps generated randomly in a 12x12x12 cm cube at the centre of two opposed arrays

(16x16 with 1 cm elements) separated by 23cm (minimum distance between points of 2cm). IBPoints+PI uses Iterative Backpropagation (200 iterations) to create focal points and then adds π radians to the phases of the top array, BPoints+PI is the non-iterative version. The x and y force stiffnesses followed similar patterns.

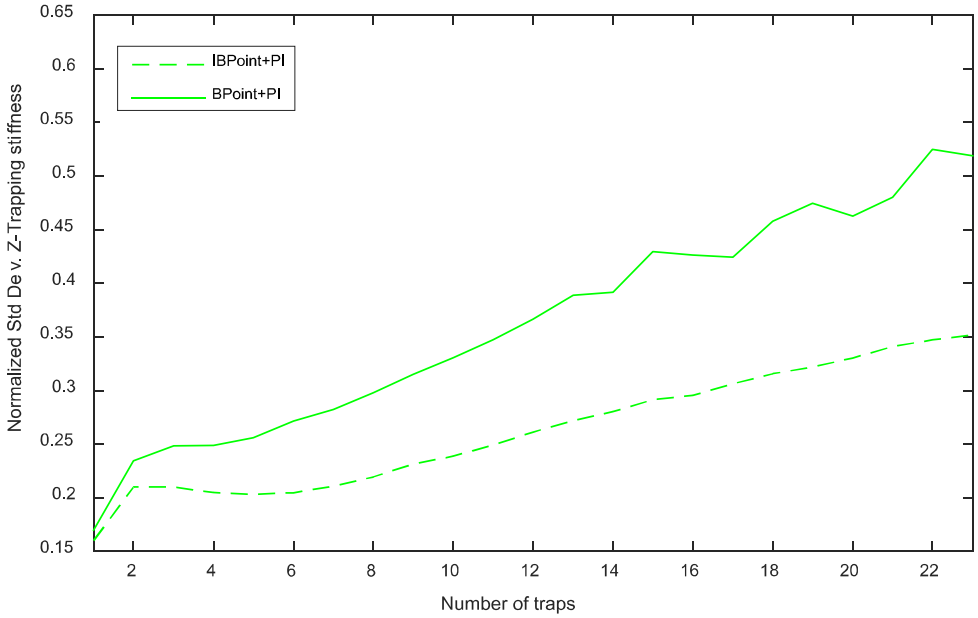

Fig. S22: Using the same data as Fig. S21, this graph shows the normalized standard deviation of trapping stiffness in the Z-direction depending on the number of traps and algorithm employed. IBPoints+PI uses Iterative Backpropagation (200 iterations) to create focal points and then adds π radians to the phases of the top array, BPoints+PI is the non-iterative version. The x and y force stiffnesses followed similar patterns.

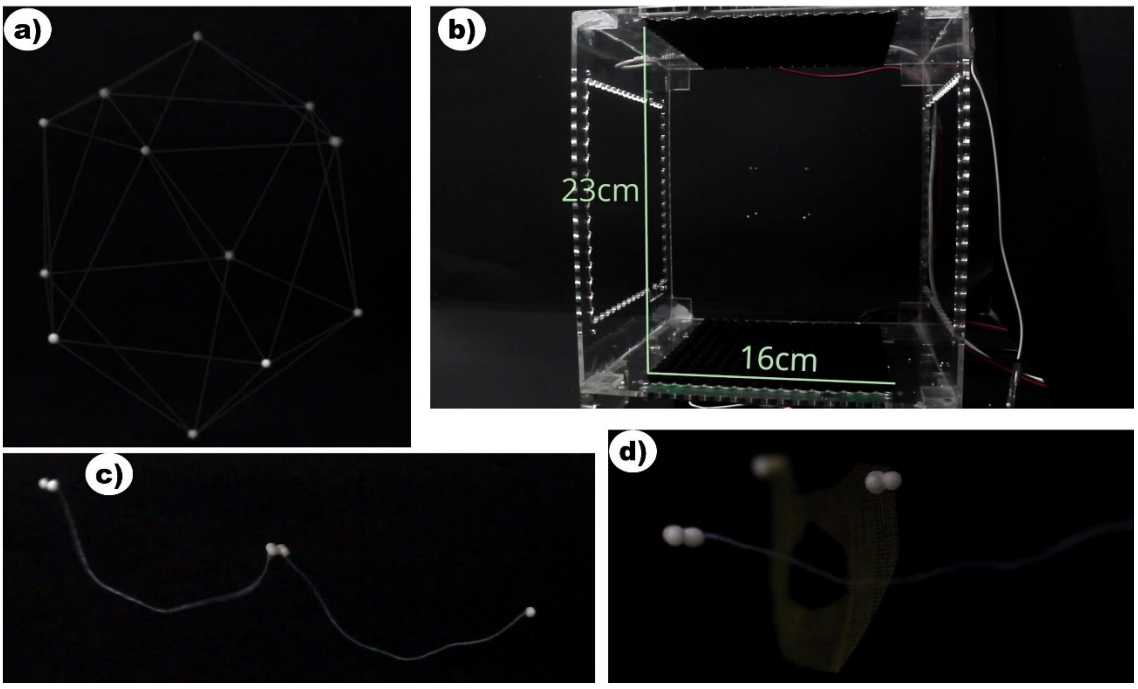

Movie S1: a) Short extracts of multiple particles being manipulated in 3D to create an icosahedron. b) The experimental setup. c) Assembly of two threads. d) Thread passed through a hole in fabric.

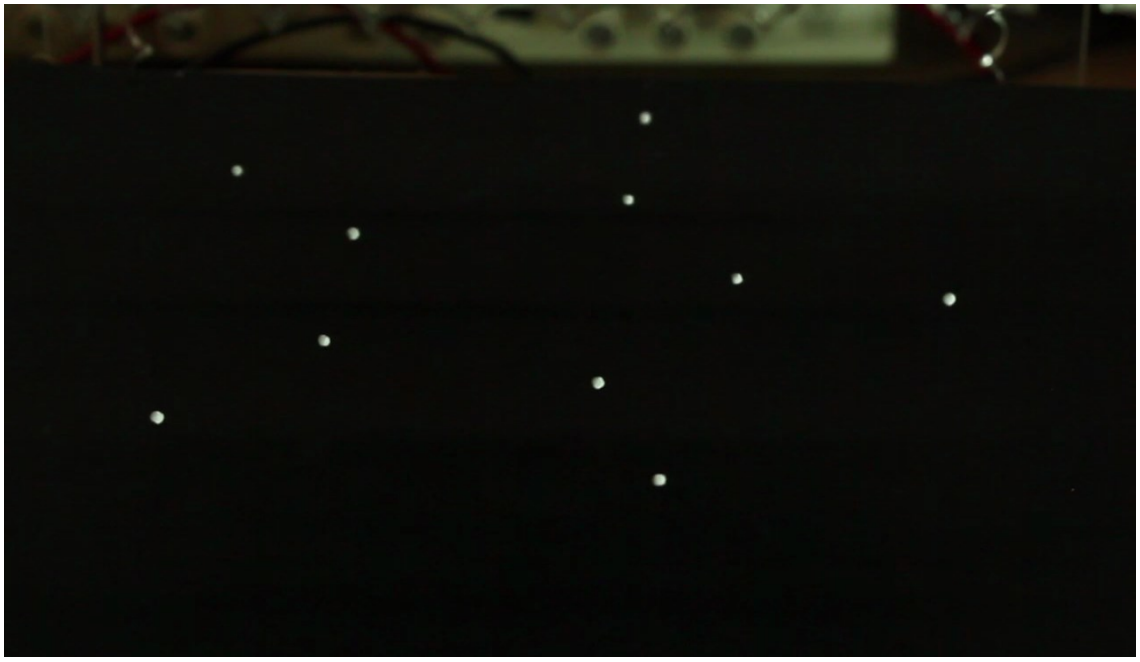

Movie S2: In-plane manipulation of 12 particles.

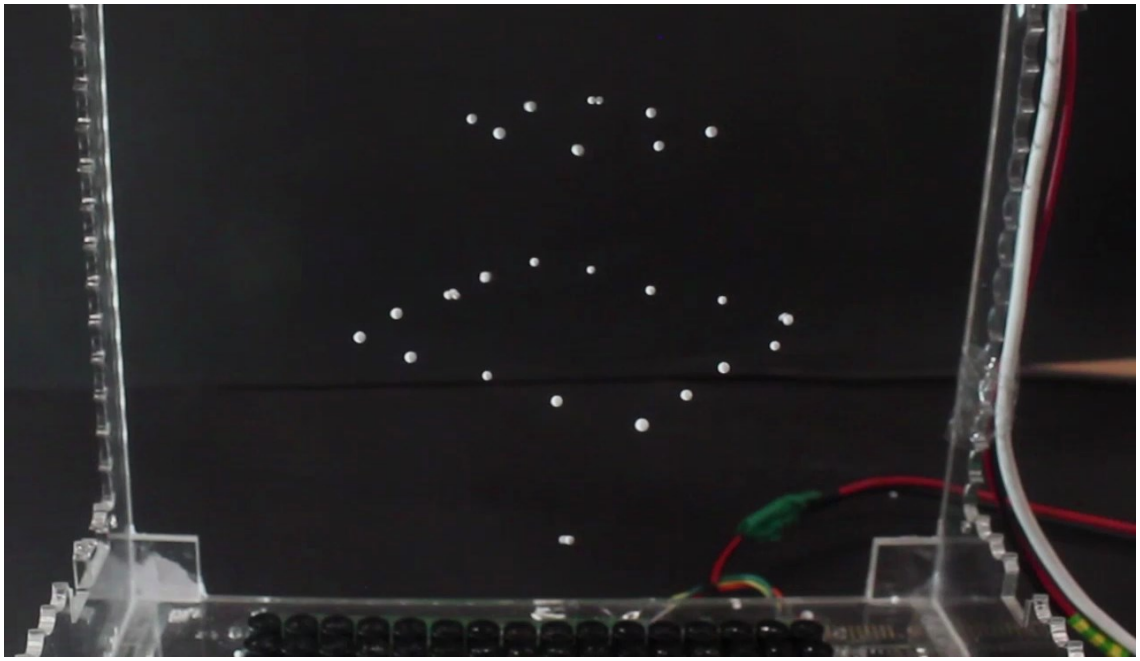

Movie S3: Manipulation of 25 particles.

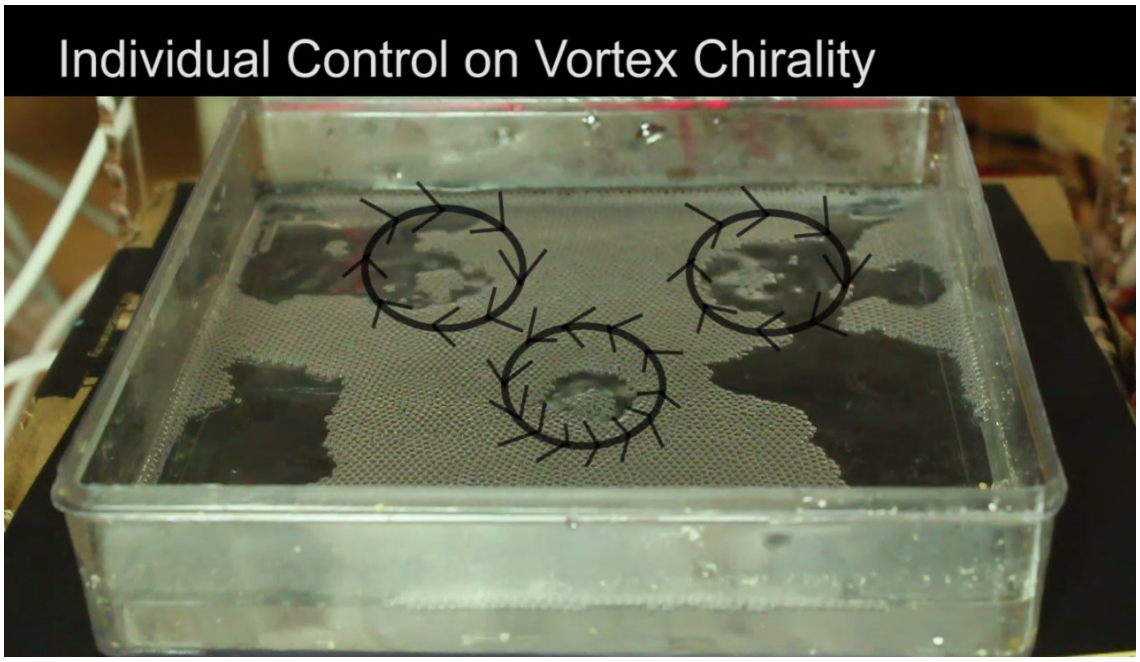

Movie S4: Generation and visualisation of 3 acoustic vortices with independent chirality.

Movie S5: Generation of 4 twin-traps with individual control on the orientation.

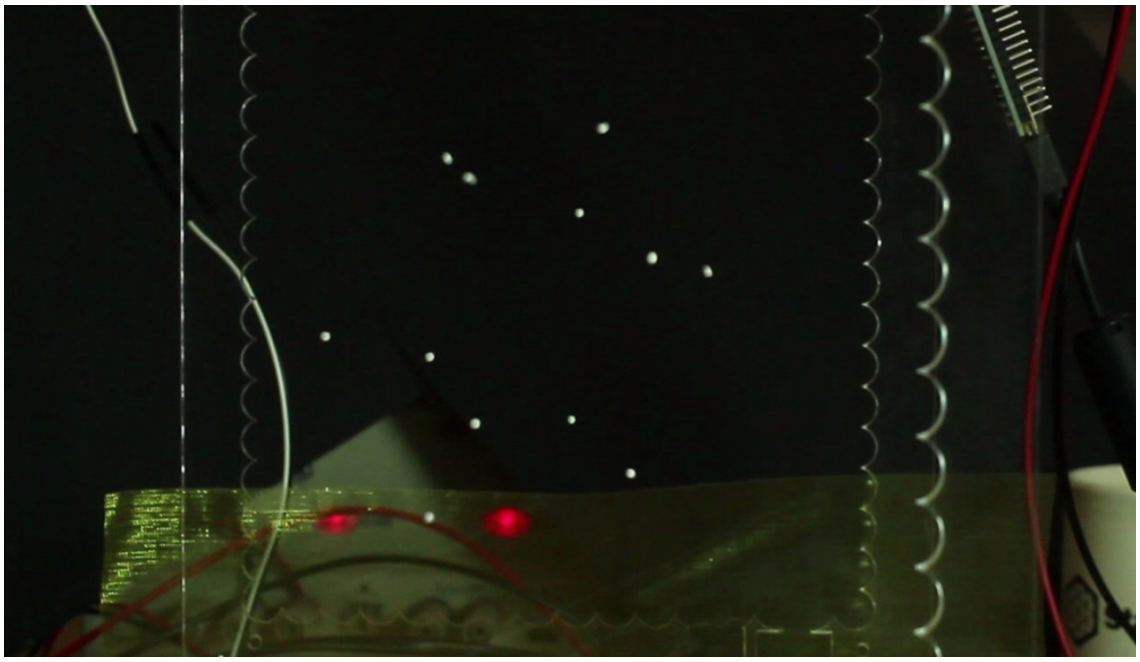

Movie S6: Trapping of 12 particles forming an icosahedron.

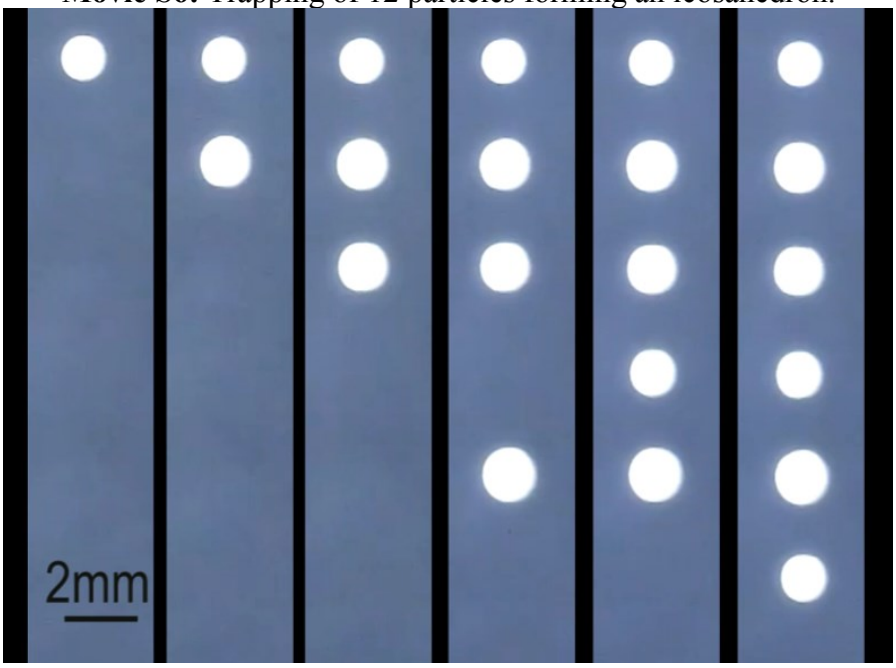

Movie S7: Placing particles in nearby nodes, no obvious disturbance was observed in the position of the other particles.

Movie S8: 1 hour timelapse of particles being levitated at the same position.

References

1. Foresti D, Sambatakakis G, Bottan S, Poulikakos D (2013) Morphing surfaces enable acoustophoretic contactless transport of ultrahigh-density matter in air. Scientific reports 3, 3176.
2. Marzo A, Barnes A, Drinkwater BW (2017) TinyLev: A multi-emitter single-axis acoustic levitator. *Review of Scientific Instruments*, **88**(8), 085105.
3. Marzo A, Seah SA, Drinkwater BW, Sahoo DR, Long B, Subramanian S (2015) Holographic acoustic elements for manipulation of levitated objects. Nature communications 6, 8661.
4. O'Neil H (1949) Theory of focusing radiators. The Journal of the Acoustical Society of America 21(5), 516-526.
5. Gor'kov LP (1962) On the forces acting on a small particle in an acoustical field in an ideal fluid. Sov. Phys. Dokl. 6, pp. 773-775.
6. Bruus H (2012) Acoustofluidics 7: the acoustic radiation force on small particles. Lab Chip 12, 1014–1021.